Influence of Aptamer Surface Coverage on Small Target Recognition: A SPR and QCM-D Comparative Study

Hannah Macdonald, Hugues Bonnet, Angéline van Der Heyden, Eric Defrancq, Nicolas Spinelli, Liliane Coche-Guerente, Jérôme Dejeu

Influence of Aptamer Surface Coverage on Small Target Recognition: a SPR and QCM-D Comparative Study

Hannah MacDonald, Hugues Bonnet, Angéline Van der Heyden, Eric Defrancq, Nicolas Spinelli, Liliane Coche-Guérente, Jérome Dejeu**

Univ. Grenoble-Alpes, CNRS, DCM UMR 5250, F-38000 Grenoble, France.

AUTHOR INFORMATION

Corresponding Author

E-mail: jerome.dejeu@univ-grenoble-alpes.fr, liliane.guerente@univ-grenoble-alpes.fr

ABSTRACT

Aptamers have emerged as promising biorecognition elements for the development of biosensors. The present work focused on the direct detection, by surface plasmon resonance (SPR) and quartz crystal microbalance with dissipation monitoring (QCM-D), of a low molecular weight (LMW) compound (less than 200 Da) with an aptamer receptor presented as an oriented monolayer on surface. These techniques are powerful for label-free, real-time characterization and quantification of molecular interactions at interfaces. Herein, we analyzed the influence of aptamer surface density on the recognition properties. A decrease of the surface

concentration was shown to improve the affinity for the target due to a higher kinetic association constant that could be explained by a limitation of the steric hindrance of the aptamer on the surface. An aptamer folding is produced upon recognition of the LMW target that gives rise to the modification of the layer on the surface. This induces a displacement of water acoustically coupled to the sensing layer, a thickness layer variation and a deviation of the refractive index increment (RII) of the target/aptamer complex from the sum of the RII of individual entities. We also demonstrated that the recognition signal was still detectable for low aptamer density (lower than 1 pmol.cm^{-2}).

INTRODUCTION

Aptamers are single-stranded RNA or DNA oligonucleotides (with a length in the range of 10-100 nucleotides) that have been developed for the recognition of various targets including small molecules, proteins and even whole cells with high affinity and selectivity.[1] They are usually selected from a combinatorial library of oligonucleotide using the Systematic Evolution of Ligands by EXponential enrichment (SELEX) process.[1] Due to their remarkable recognition properties, the aptamers have emerged as promising biorecognition elements in the development of biosensors (i.e."aptasensors" for aptamer-based biosensors), and are now considered as a valuable alternative to antibody-based sensors.[2-4] The grafting of the aptamer onto a solid support requires its functionalization by a suitable functional moiety depending on the immobilization procedure. This is a crucial point as the attachment method could have a great influence on the affinity of the aptamer for its target and consequently on the sensitivity of the biosensor. Indeed, non-specific interactions of the aptamer with the surface or limitation of the binding site accessibility due to proximity towards the surface[5-7] or steric hindrance induced by high surface

density[8, 9] can lead to a loss of affinity. It has been reported that the aptamer orientation, spacer length (between aptamer and anchoring moieties) and electrical charge of the surface have influence on aptamer microarray performance for the detection of fluorescently labeled compound,[6, 7] as also suggested by dynamic molecular simulation.[5] Martin et al. demonstrated that an oligothymidylate linker is a consistent choice for linker across different types of aptamer/target pairs and approximately 10 nucleobases are required to increase the sensitivity of the response without affecting the affinity.[7]

We recently reported the study of a new aptasensor, which binds enantioselectively a low molecular weight compound using saturated aptamer layer.[8, 9] In the surface plasmon resonance (SPR) study, a higher signal was obtained compared to the one expected for the target recognition as proposed by Wilson and David's formula.[10] To explain this phenomenon, a new model was developed to identify the contribution of the aptamer conformational transition to the signal. In addition to the reduction of the sensing layer thickness, the model highlighted the non –additivity of refractive indexes increment (RII) for this recognition system: the RII value of the recognition complex is not equal to the sum of the RII values of two initial partners.[9] This non – additivity of the RII for the complex was already measured by Bornhop[11] et al. in solution but never revealed on surface. The recognition was also monitored using quartz crystal microbalance with energy dissipation (QCM-D)[8] and similar affinity constants were measured around 100 μM for both technics. However, these values are two orders of magnitude compared to affinity measured in solution (1-3 μM).[12-14] The immobilization being performed using saturated surface of biotinylated aptamer on a streptavidin platform, we hypothesized that the aptamers crowding should hamper the folding (necessary for recognition[13]) leading to a decrease of the affinity. The notion of surface probe density has been approach for the elaboration of electrochemical

aptasensors via the direct coupling of aptamer through a thiolate or phosphoamidate anchoring function.[15, 16] Ceretti et al. reported an optimized surface densities for the signal generated by the capture of radiolabeled target.[15] In the case of redox tagged aptamer, White et al. studied the effect of the surface density on the response of their electrochemical aptasensors.[16] However, to the best of our knowledge, no systematic study of the impact of aptamer surface densities on the affinity of the interaction has been reported to date. In the present article, we report on the influence of the aptamer surface coverage on its affinity for a small target and in particular its kinetic evaluation. We also confirmed that the non –additivity of refractive indexes increment (RII) for this recognition, previously observed for saturated aptamer density, was not induced by steric hindrance and was present whatever the aptamer density.

Materials and Methods

Chemicals

Tris(hydroxymethyl)aminomethane (Tris), (11-mercaptoundecyl)tetra(ethylene glycol) HS-(CH2)11-EG4-OH, MgCl2, NaCl, L-tyrosinamide and streptavidin, were purchased from Sigma-Aldrich. Polyoxyethylene sorbitan monolaurate (Tween 20®) was purchased from Euromedex, absolute ethanol was purchased from Acros, (11-Mercaptoundecyl)hexa(ethylene glycol) biotinamide HS-$(CH_2)_{11}$-EG_6-biotin was purchased from Prochimia (Poland). All aqueous solutions were prepared by using ultrapure water (Purelab UHQ) filtered (0.2 μm pore size). Experiments were performed in Tris buffer (20 mM Tris, 50 mM NaCl, 5 mM $MgCl_2$, 0.05% v/v Tween 20®, pH=7.5 in water). The oligonucleotides sequences were prepared as previously described.8 Their sequences are the following: L-Tym aptamer (Apt_{49}), $^{5'}$AAT TCG CTA GCT

GGA GCT TGG ATT GAT GTG GTG TGT GAG TGC GGT GCC C $X^{3'}$ and random DNA sequence, $^{5'}$TGA TCA GAT GAG CGT TCC CAG CAC TTC AGC CGA CGA TGC AAC CAG TTT T $X^{3'}$, in which X represents the 3' biotin triethylene glycol (TEG). Aliquots of oligonucleotides were dissolved in water and stored at - 20°C. Before each measurement, the solutions of aptamer or random DNA sequence were prepared in Tris buffer, heated 5 minutes at 90°C and cooled overnight at room temperature.

Sensor Chip surface generation

Upon removal from storage in fridge, bare gold sensor chip was rinsed with ultrapure water, dried in a nitrogen gas stream and exposed for 10 min to UV-Ozone cleaning (Model 42-220; Jelight Conpany Inc.). The cleaned gold surface was then dipped overnight in the mixture solution of thiols (90% of 1mM HS-$(CH_2)_{11}$-EG_4-OH and 10% of 1mM HS-$(CH_2)_{11}$-EG_6-biotin) in ethanol. Next, the surface was carefully cleaned with ethanol and dried with gaseous nitrogen. It has been demonstrated that 10% of biotinylated thiol is necessary to obtain a streptavidin layer with maximum surface coverage.[17] The functionalized gold sensor chip was mounted on the sample holder for immediate usage using QCM-D or SPR. All the experiments were performed with a saturated streptavidin layer and the aptamer density was controlled by the aptamer injection time and concentration. Indeed, this stratified system offers the selective immobilization of molecules (protein, DNA, …) with well-controlled orientation and density. [18-20]

Surface Plasmon Resonance Measurement

All SPR measurements were performed at 25°C in a four flow-cell Biacore T200 instrument (GE Healtcare). The experimental conditions were similar to the previous reported.10 Briefly,

streptavidin (50 µg mL^{-1}) was injected on the biotinylated surface at 30 µL.min^{-1} for 15 min. Random DNA sequence and aptamer solutions were then injected, into the reference and sample channels respectively, at a flow rate of 2 µL.min^{-1}. The injection time of the oligonucleotide sequences was adjusted to control their areal density. L-tyrosinamide solutions, with different concentration, were injected for 2 min at a flow rate 30 µL.min^{-1} and the flow-cells were then rinsed with the running buffer during 3 min. The value of the signal was measured 4s before the end of the L-tyrosinamide injection. The signal recorded on the scramble reference channel 1 was subtracted from the signal of the sample channel 2, 3 and 4 by applying a double-referencing procedure: correction of the device drift and of the refractive index difference between the RB and the injected solutions.[21]

Quartz Crystal Microbalance with Dissipation Monitoring (QCM-D) Measurements

QCM-D measurements were performed using Q-Sense E1 or E4 instruments (Biolin Scientific) equipped with one or four flow modules, respectively. Besides measurement of bound mass, which is provided from changes in the resonance frequency, *f*, of the sensor crystal, the QCM-D technique also provided structural information of biomolecular films via the changes in the energy dissipation, *D*, of the sensor crystal. f and D were measured at the fundamental resonance frequency (4.95 MHz) as well as at the third, fifth, seventh, ninth, eleventh, and thirteenth overtones (i = 3, 5, 7, 9, 11 and 13). Normalized frequency shifts $\Delta f = \Delta fi/i$ and dissipation shifts $\Delta D = \Delta Di$ were presented.

Experiments were conducted in a continuous flow of buffer with a flow rate of 50 µL.min^{-1} by using a peristaltic pump (ISM935C, Ismatec, Switzerland). The temperature of the QCM-D

platform and all solutions were stabilized at 24°C to ensure stable operation. All buffers were previously degassed in order to avoid bubble formation in the fluidic system.

In the case of homogeneous, quasi-rigid films, the frequency shifts are proportional to the mass uptake per unit area (mQCM), which can be deduced from the Sauerbrey relationship:[22]

$$m_{QCM} = - C.\Delta f \quad (1)$$

where the mass sensitivity, C, is equal to 18 $ng.cm^{-2}.Hz^{-1}$ at f_1 = 4.95 MHz. It should be kept in mind that if the film is solvated, the acoustic areal mass density of the film will be composed of the areal mass densities of the adsorbate, mads, and the hydrodynamically coupled solvent, $m_{solvent}$:

$$m_{QCM} = m_{ads} + m_{solvent} \quad (2)$$

In the case of soft films ($\Delta D > 0$), the adlayer was modeled as a homogeneous layer of thickness d_{QCM} and density ρ, using a continuum viscoelastic model (See equation S1).[23]

Results and Discussion

Quartz crystal microbalance (QCM-D) studies.

The anchoring of the oligonucleotides (i.e. L-Tym aptamer and scramble) was achieved through streptavidin-biotin interactions (see materials and methods). The self-assembled monolayer of pegylated alkane thiols bearing hydroxyl and biotin groups was first performed ex situ. The formation of the subsequent biomolecular layers was monitored using QCM-D. After equilibration of the QCM-D signals (f and D) in the running buffer, the streptavidin (SA) was injected in the measurement chamber until reaching saturation of the QCM-D signals. As

previously reported,[8] the immobilization of SA led to a change in frequency closed to -22 Hz (Figure S1) whereas the change in dissipation was very low indicating the formation of a rigid layer. By using Sauerbrey equation, the shift in f is converted in hydrated mass mQCM(SA) = 396 ng.cm^{-2}. This value is as expected for the formation of rather dense protein monolayers.[8] The biotinylated aptamer Apt_{49} was adsorbed onto the SA platform for which the average molecular surface density was controlled by the time of injection. A roughly linear relationship between the molecular surface density ΓApt49 and the frequency shift was reported from QCM-D ellipsometry coupling experiment. A conversion factor of – 5.95 Hz cm^2.pmol^{-1} was obtained that allows the quantification of the surface density of the aptamer from QCM-D frequency shifts.[8] Several functionalized surfaces were prepared with frequency shifts ranging from - 4 to - 33 Hz (Table S1) corresponding to aptamer molar surface densities of 0.7 to 5.5 pmol.cm^{-2}. The Apt_{49} layer could not be considered as a rigid layer as the changes in energy dissipation varied from 0.7 to 2.7 10^{-6}. The QCM-D signals measured at several overtones i, could provide quantitative information, in particular the acoustic areal mass density (mQCM which includes hydrodynamically coupled solvent) but the application of the viscoelastic modeling requires a sensing layer, which behaves as a homogenous film. At low surface coverage we could probably not make the hypothesis of a homogeneous film of aptamer because the oligonucleotide behaves as hydrated discrete particles distributed through the SA platform.[14] Nevertheless, we could make an estimation of the acoustic mass m_{QCM} using the QTM software (See SI for results for modeling with QTM and Figure S2) and calculate the hydration ratio by the following relation: $H\% = (m_{QCM}-m_{SE})\times 100/m_{QCM}$, (See Figure S3), m_{SE} is the optical mass calculated from Δf by using the factor: - 5.95Hz.cm^2.pmol^{-1} previously reported and an aptamer molecular weight of 15 831 g mol^{-1}.[8] The calculation revealed a degree of hydration varying from 88% (for high surface

coverage) to 93% (in the case of low surface coverage), such high hydration ratio have ever been reported for DNA films.[24, 25] The decrease of coupled water induced by lowering the surface coverage as sensed by QCM-D has been reported and modeled for globular proteins, virus particles and small unilamellar vesicles.[26] The authors showed that the hydration curves could be reproduced quantitatively using a model that ascribed a hydration coat (truncated pyramid-shaped) to each adsorbed particle. We reported previously that the low thickness of the saturated aptamer layer suggests that the strands did not adopt an elongated structure but were presented in a coiled conformation.[8] The surface area ranged from 30 nm² to 300 nm² per Apt_{49} (Figure S4), corresponding to an average spacing from 19.5 nm to 5.5 nm (Figure S5), respectively (assuming packing in a square, circular polymer-like chain arrangement). The ligand spacing distance of 5.5 nm determined for the highest surface coverage is closed to the gyration radius of Apt49 (Rg = 4.7 nm calculated from the hydrodynamic radius of Apt49 Rh = 3.3 ± 0.1 nm per Apt49 measured by Dynamic Light Scattering, see SI).[27, 28]

The recognition properties of the Apt_{49} sensing layer have been analyzed by the transient exposure of the aptasensors to various concentrations of *L*-Tym ranging from 5 nM to 1 µM. We previously demonstrated the selective response of the Apt_{49} sensing layer by the absence of QCM-D response of a random DNA sequence.[8] The QCM-D responses of aptasensors bearing various surface coverages upon exposure with 1mM *L*-Tym are depicted in figures 1 and Figure S6.

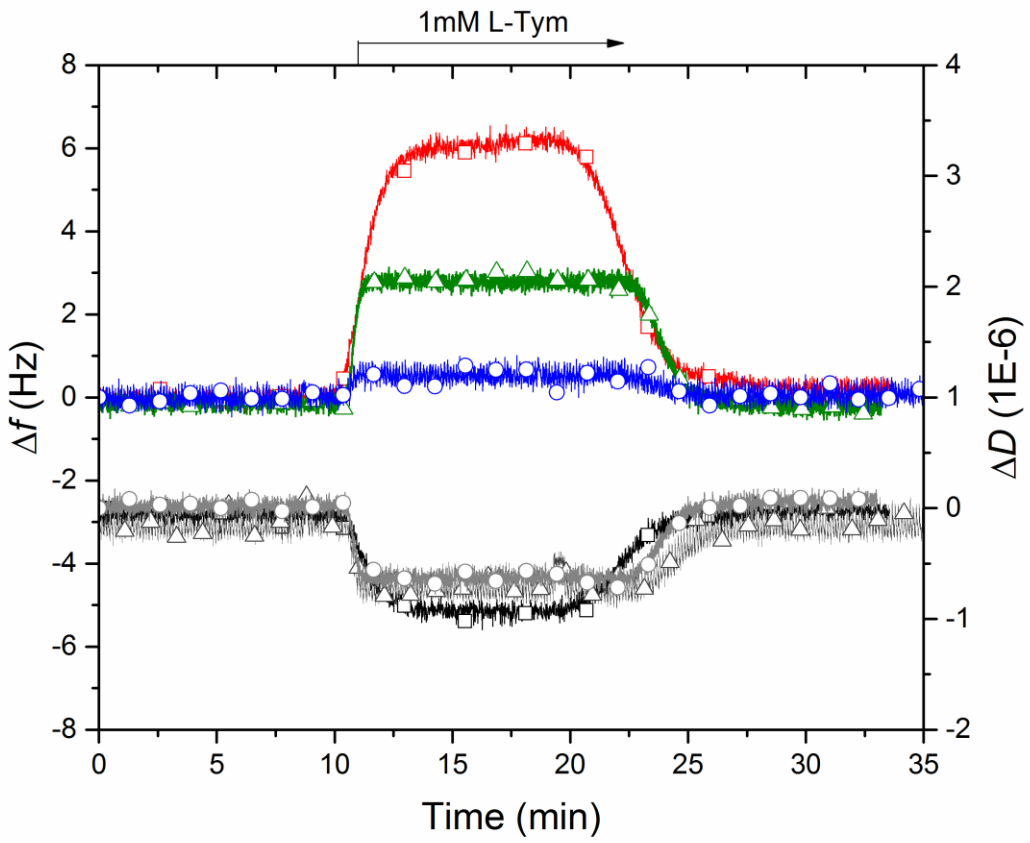

Figure 1: QCM-D signals recorded during injection of L-Tym 1mM onto various sensing aptamer layers exhibiting different surface densities: (▫) red (Δf) and black (ΔD) signals for 4.3 pmol.cm^{-2} of aptamers; (Δ) green (Δf) and dark grey (ΔD) signals for 2.9 pmol.cm^{-2} of aptamer and (○) blue (Δf) and light grey (ΔD) signals for 0.7 pmol.cm^{-2} of aptamer. The arrows represent the start and duration of injections. f and D variations for the 3rd overtone are shown; T = 24°C, flow rate = 50 µL.min^{-1}.

As previously reported,[8] the recognition of the target molecule is identified by a frequency increase and a dissipation decrease. These variations were specific of the recognition since signal variations were not observed upon target injection on streptavidin alone and on a random DNA

sequence immobilized on the same SA platform. Moreover, the recognition is enantiomeric as no frequency and dissipation variations were recorded upon D-Tym injection.[8] The QCM-D signals variation demonstrated a loss of mass (positive shift in *f* and negative shift in *D*), which was attributed to a dehydration of the aptamer layer associated to a change in the conformation of the oligonucleotide on the surface upon recognition of the target molecule.[8] In the present study, the dehydration was found to be dependent of the Apt_{49} surface coverage and consequently the positive shifts in *f* measured during the recognition event were also dependent on the Apt_{49} surface coverage (See Figure S6).

We previously reported that the K_D value determined from the values of shifts in frequency was similar to that determined from the change in acoustic mass corresponding to a loss in water mass.[8] In the present study, for low surface coverage, the calculation of the change in acoustic mass from the viscoelastic modeling was not relevant because of film inhomogeneity. The determination of K_D, considering a 1:1 binding stoichiometry, was based on the direct measured Δf resulting from the injection of increased concentrations of *L*-Tym from 5 nM to 1 µM (See Figure S7). These K_D values should be considered as apparent K_D (noted K_{Dapp}) as they were indirectly obtained from the quantification of the expelled water upon *L*-Tym binding and not to the added mass of *L*-Tym trapped by the aptamer layer. Figure 2 shows the evolution of the apparent K_D values as a function of the average spacing between two aptamers (determined from surface coverage, see SI). The K_{Dapp} values ranged from 160 µM for the lowest interligand distance (i.e. highest surface coverage) to 13 µM for the highest interligand distance (i.e. lowest surface coverage).

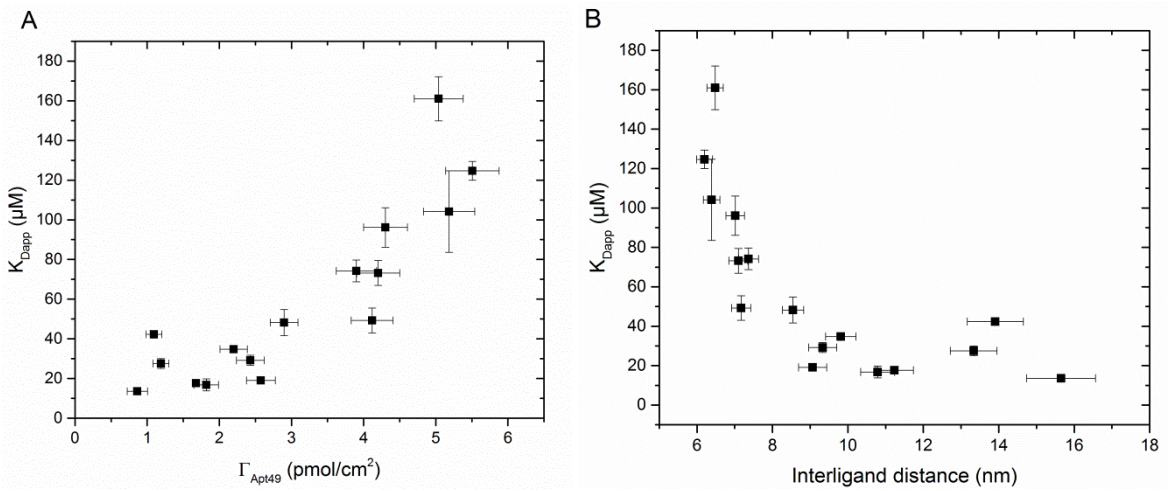

Figure 2: Plot of apparent K_D (determined by the shifts in frequency for concentrations in L-Tym ranging from 5nM to 1µM) as a function of A: aptamer surface coverage and B: the average spacing between Apt_{49} grafted onto the 2D SA platform (the average spacing were determined from the surface coverage assuming packing in square lattice, see SI).

We noticed a quasi-exponential increase of the apparent KD as a function aptamer surface density. The affinity was thus improved when the surface coverage was decreasing, figure 2.A (i.e. increase of the interligand distance between Apt_{49} receptors, figure 2.B). This observation was correlated with the steric hindrance induced by the saturation of the aptamer layer on the 2D platform of SA, which should hamper the conformational change of the aptamer upon L-Tym binding. Indeed, for high surface coverage, the KDapp values are about two orders of magnitude higher than those measured by homogeneous techniques such as isothermal calorimetry (1.75-3.2 µM),[12] fluorescence polarization (1.7-2.2 µM)[13] or electrochemistry (2.9 µM).[14] In contrast, for lower surface coverage the apparent K_D values are higher of only one order of magnitude. We can assume that the folding of the aptamer upon recognition is less hampered thanks to a higher degree of freedom on the surface for low than for high coverage. These difference with

experiments performed in solution could be explained by the limitation of the access of the target to the binding site in close proximity to the surface.[5-7] While some recognition systems led to similar affinity[29, 30]analyzed from binding assays performed in homogeneous solution or from current immobilized ligand-based assays, several studies exhibited discrepancies between these methods and a lower affinity constant is usually measured by surface sensitive techniques because the affinity could be affected by the grafting of the ligand to the surface.[5, 7, 31-34] In our case, similar results could probably be obtained if measurable signals were obtained at lower aptamer density (< 0.7 pmol.cm^{-2}). From figure 2, we could observe a threshold value of aptamer density of about 2.5 pmol.cm^{-2} (ligand spacing of about 9 nm) below which, K_{Dapp} values were constant (26 ± 8 µM). This interpretation is supported by the work of Heinen et al. who calculated the anchor distances, d, between two polymer chains on gold surface and the degree of chain overlap for poly(glycidyl ether) copolymers. They classified the polymers conformation through different regimes, brush-like with extensive chain overlap for $d \leq Rg$ (Rg stands for gyration radius) or overlap without open space for $d \leq \sqrt{2}Rg$ and mushroom-like with beginning of overlap with open space for $d \leq 2Rg$ or no overlap for $d \geq 2Rg$. In our case, the transition between brush-like and mushroom-like with no overlap would occur around 9 nm, a value closed to 2 Rg = 9.4 nm. That demonstrates the influence of aptamer surface density on the Apt_{49}/L-Tym interaction and emphasizes the necessity to preserve the aptamer flexibility. In addition, the aptamer surface density must be optimized for the development of aptasensors by taking into account the sensitivity of the transducing technique. Indeed, the decrease of aptamer surface coverage should be accompanied by a decrease of the QCM-D response, which is connected to a loss of water hydrodynamically coupled to the sensing layer. When the aptamer surface coverage is too low, the loss of water should reach a mass below the detection limit of

the technique. The optimization of the aptamer surface density thus results from a compromise between a sufficiently high sensitivity of detection and a low overlapping of the oligonucleotides onto the functionalized surface.

Surface Plasmon Resonance Study.

To further analyze the influence of the aptamer surface density on the aptamer/*L*-Tym interaction SPR studies were also performed. This optical technique allows to sense directly the amount of target molecule trapped by the aptamer layer. The affinity of *L*-Tym for the aptamer immobilized with various surface coverages was explored using the same recognition platform as the one used for QCM-D study. The aptamer and random DNA sequence monolayers were immobilized through streptavidin-biotin interactions using a saturated SA layer formed on the 10% biotinylated self-assembled monolayer. The surface density of aptamers was controlled using different times of injection and correlated to the SPR signal variation, expressed in Response Unit (RU).[10] This experimental signal could be converted in aptamer surface density with the Jung's relationship (Eq. S5).[35]

The recognition of L-Tym for the different aptamer density was evaluated at different surface densities of aptamers (R.U. values from 50 to 600 corresponding to 0.33 to 4 pmol.cm^{-2}). L-Tym solutions ranging from 250 nM to 1mM were injected on the aptamer layers exhibiting various surface densities (see sensorgramms on Figure S8). The signals, obtained on the reference flow-cell, were proportional to the analyte concentration and independent of the random DNA surface density. These variations were thus assigned to the refractive index variation of the injected target solutions.[9] Moreover, no recognition signal was observed on the active flow-cell when the enantiomeric conformation of the target, D-Tym, was injected, whatever the aptamer density

(Figure S9). Therefore, the double-reference subtracted signal was specific of the target recognition by the aptamer layer.

Sensorgrams were obtained after subtraction of the signals recorded on the random oligonucleotide layer from the one recorded on the aptamer layer by applying a double referencing procedure. As previously reported,[9] a specific signal for the L-Tym recognition was obtained. The interaction was completely reversible and no regeneration step was necessary. On Figure 3, sensorgrams recorded for injection of L-Tym at 1mM are overlaid for several surface densities in aptamer.

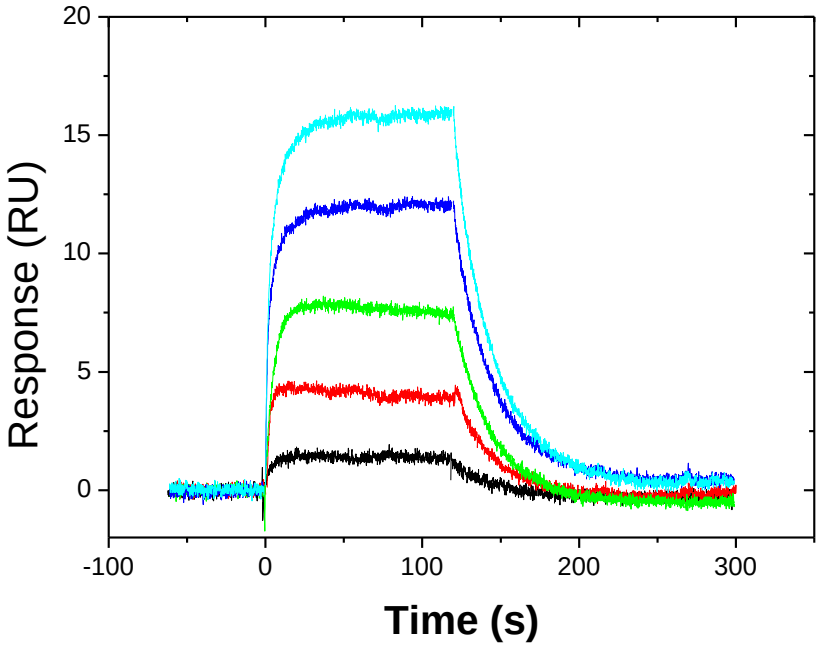

Figure 3: SPR double-reference subtracted sensorgrams recorded during the interaction of L-Tym 1 mM with surfaces presenting different aptamer surface densities: Signal recorded during the aptamer immobilization are 0.33 pmol.cm^{-2} (black), 0.76 pmol.cm^{-2} (red), 1.33 pmol.cm^{-2} (green), 1.84 pmol.cm^{-2} (blue) and 2.86 pmol.cm^{-2} (blue cyan). T= 25°C, Flow rate: 30 µL.min^{-1}.

It is noteworthy that despite the low molecular weight of the target, its interaction with the aptamer 2D platforms led to measurable signals even for low aptamer densities. After double-referencing procedure, the maximum signal (RUmax) recorded for injection of 1µM L-Tym solution varied from 1.7 RU (for an aptamer density of 0.33 pmol.cm^{-2}) to 17 RU (for an aptamer surface density of 4 pmol.cm^{-2}) as represented on Figure S11. For each aptamer density, the signal intensity evolved in a close-dependent manner with the L-Tym concentration in solution. The obtained sensorgrams thus allowed the determination of the equilibrium dissociation constant (Figure S10) of the interaction from the responses obtained at the steady state (Req) or from the kinetic constants based on a 1:1 interaction model. For both methods, the determined KD values were similar for each aptamer surface coverage (Figure S10). K_D values decreased from 120 to 20 µM as the interligand distance increased confirming the influence of steric hindrance. The values of KD obtained from both techniques (QCM-D and SPR) were found similar at low coverage.

The analysis of kinetic association and dissociation rates, k_{on} and k_{off}, respectively can give useful information on the recognition process on surface (Figure 4).

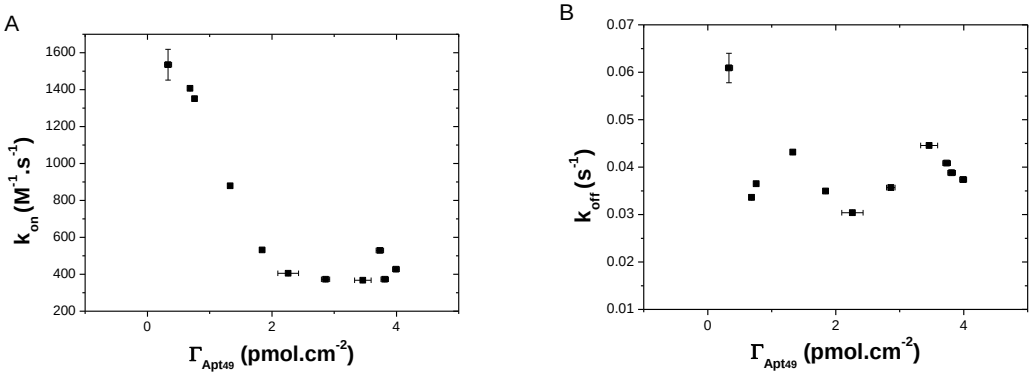

Figure 4: Variation of the kinetic parameters of the interaction as a function of the aptamer density. A) variation of association kinetic rate $k_o n$, B) variation of the dissociation kinetic rate k_{off}.

No significant influence of the aptamer surface density on k_{off} was observed (average value of 0.04 s-1), whereas the kinetic association rate (k_{on}) was found to increase with the interligand distance. Indeed at low coverage, k_{on} value was close to 1500 M-1.s-1 and decreased 3.5 fold (around 400 M-1.s-1) at aptamer surface saturation. The affinity increase was thus due to a faster recognition of the L-Tym by the aptamer at high interligand distances. This process was favored by using a low aptamer density, which does not impede the aptamer folding. These results suggest that the critical step for the recognition of the L-Tym by the aptamer is the association step, which could be disrupted by an important aptamer coverage so when the strands hinder each other.

Non –additivity of the complex RII

We have previously reported that the maximum response obtained experimentally upon recognition at saturated aptamer coverage (17.9 RU) was higher than the theoretical one (7.9 RU) obtained from the Davis and Wilson's relationship[10]:

$$R_{A_{max}} = RU_L \frac{MW_A.\left(dn/dc\right)_A^{'}}{MW_L.\left(dn/dc\right)_L^{'}} \times V = \beta.RU_L \times V \qquad (3)$$

Where R_{Amax} is the expected maximum response, RU_L is the aptamer immobilization level, MW_A and MW_L are the molecular weights of the injected analyte (*L*-Tym, 180.2 g.mol^{-1}) and of the immobilized ligand (aptamer, 15 831 g.mol^{-1}), respectively. $\left(dn/dc\right)_A^{'}$ and $\left(dn/dc\right)_L^{'}$ are the

refractive index increments (RII) for the analyte (*L*-Tym, 0.219 $cm^3.g^{-1}$)[9] and for the ligand (aptamer, 0.176 $cm^3.g^{-1}$)[36-38] respectively. $\beta = MW_A.(dn/dc)'_A / MW_L.(dn/dc)'_L$ is the ratio of the mass-weighted RII of the analyte *versus* the ligand and the *V*, the valency *i.e.* the ratio number of analytes *per* number of ligands involved in the recognition (*V*=1 in the present system).

This observation was confirmed for all surface coverages (see Figure S11 and Figure 5). We have demonstrated that the amplification of the signal (compared to the theoretical one) is attributed only partially to the sensing layer thickness decrease of the surface that occurs upon aptamer folding (around 25 %) and majorly to the aptamer-*L*-Tym complex RII deviation from the sum of the RII of the individual entities.[9] This RII deviation, expressed with a correction factor x of the aptamer RII, could be triggered by the conformation transition of the aptamer upon recognition to the *L*-Tym. Such RII deviations were also reported from backscattering interferometry measurement, for recognition systems undergoing significant conformation or hydration changes.[11] As demonstrated by QCM-D and QCM-D-SE experiments, upon *L*-Tym recognition, the aptamer sensing layer undergoes both a reduction of its thickness and a decrease of its hydration ratio.

While the RII value of the aptamer was 0.176 $cm^3.g^{-1}$ before the recognition, we have demonstrated that this parameter was increased by 1.48% during the recognition with *L*-Tym.[9] The SPR signal is influenced by i) the analyte binding, ii) the modification of the sensing layer thickness (corresponding to the folding of the aptamer) and iii) the RII deviation of the recognition complex. Considering the latter parameters, we have proposed a new evaluation of the theoretical maximal response using Dejeu et al.'s equation[9]:

$$RU_{A_{max}} = RU_L \left(\frac{1}{\rho} \frac{1 - e^{-\frac{\rho d_L}{d_p}}}{1 - e^{-\frac{d_L}{d_p}}} (\beta \times V + 1 + x) - 1 \right) \quad (4)$$

Where $\boldsymbol{d_p}$ is the effective penetration depth of the SPR wave (175 nm), $d_{L\ is}$ the sensing layer thickness before the analyte recognition, $\rho = d_{LA}/d_L$ is the thickness variation ratio of the sensing layer with d_{LA} the sensing layer thickness during the analyte recognition, and x is the ligand RII correction factor due to its interaction with the analyte.

Based on this equation, the RII variation was calculated for each aptamer layer displaying different surface coverage. As suggested by the similar k_{off} values calculated for the recognition occurring at various aptamer surface coverage (Figure 4B), we assumed that the folding ratio of the aptamer is constant to 0.73. Figure 5 highlights the contribution of the aptamer conformational transition to the SPR signal.

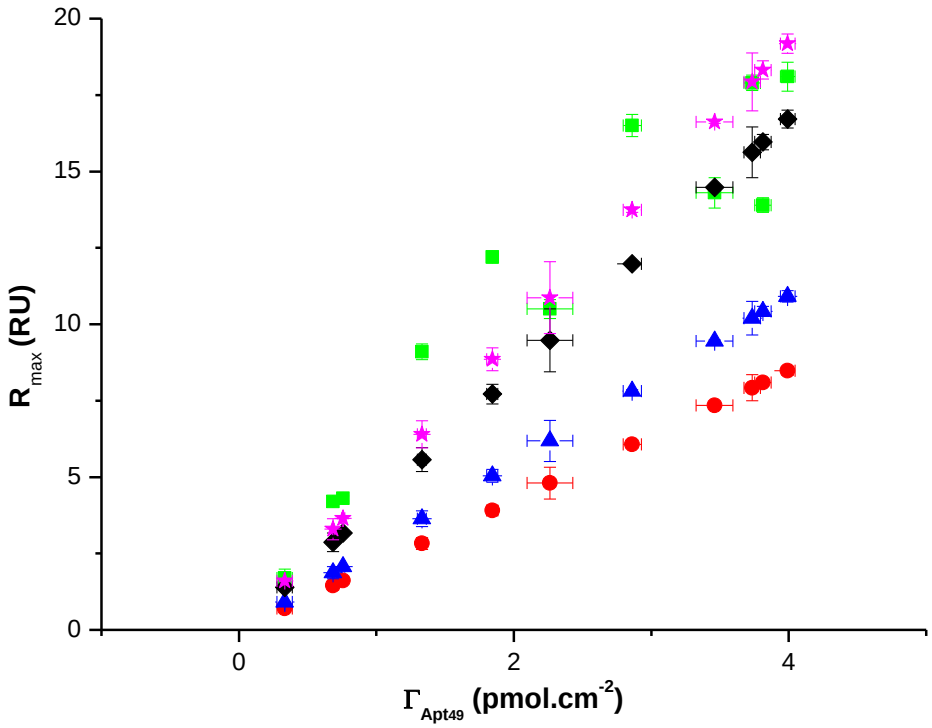

Figure 5: Comparison of the maximal response (green square) experimentally measured, RU_{Amax}, (red ring) expected from the Davis and Wilson's relationship[10] and (pink star) expected from Dejeu et al. relationship[9]. The latter relationship, in addition to the target recognition takes into account modification of the physical parameters of the complex L-Tym/aptamer: (blue triangle) folding alone, (black diamond) RII correction alone and (pink star) folding and RII correction. Calculation were made with dp=175nm, d_L=5.2 nm, ρ=0.73, β= 0.012 and x=0.01369.[9]

It should be noted that for all surface coverages, the decrease of the sensing layer thickness induced by the aptamer folding increased the expected signal by a factor 1.3 and was not sufficient alone to fit with the experimental values. If we consider only the RII correction without aptamer folding, the expected signal increased twice, and was slightly inferior to experimental one. This observation confirms that, in our case, the aptamer folding is not the main

source of the SPR signal enhancement. A better correlation between the experimental and theoretical values is observed when taking into account all these parameters (RII correction and folding). These experiments highlight that the major contribution of the SPR response is the target recognition and the RII correction and that this latter parameter should not be ignored when studying LMW target recognition. To date, signal enhancement have been seldom observed and reported for proteins undergoing target-induced conformational change. The authors ascribed the amplification to modification of the protein hydrodynamic radius upon recognition. In the present study, we confirmed that in the case of low molecular weight analyte recognition by receptor undergoing conformational, signal amplification mainly originates from the non-additivity of RII. [39,40]

Conclusion

In this paper, we studied the influence of the aptamer surface density on the recognition of a low molecular weight analyte by its receptor presented as a 2-D monolayer. Despite the low density of the ligand (from 5.5 to 0.7 pmol.cm^{-2}) and low molecular weight of the analyte (180 Da), significant SPR and QCM-D signals were observed. Indeed, at the lower coverage, even if the signals did not exceed 2 RU for SPR and 0.5 Hz for QCM-D the quantification of the interaction could be performed. We observed that the equilibrium dissociation constant decreased when the aptamer surface coverage decreased. By SPR, we demonstrated that this is due to a higher kinetic association rate whereas the kinetic dissociation rate remained constant whatever the aptamer surface density was. The aptamer spacing improved the recognition until a minimal value of 9 nm. This minimal distant is necessary to not disturb the aptamer folding and the mass water

expelling. The aptamer conformational transition induced an unexpected enhanced SPR signal compared to the one expected from the Wilson and Davies relation. The experimental SPR signal was found higher not only thanks to the folding of the aptamer but also thanks to a deviation of the analyte/receptor complex RII from the sum of the two initial partners RII. By taking into account these two parameters using the Dejeu's relationship, a good concordance was found between the experimental and the theoretical SPR values for all aptamer surface coverage and was not induced by steric hindrance (present whatever the aptamer density). A higher influence of the RII variation on the SPR signal was demonstrated compared to the increase due to the sensing layer thickness variation.

ASSOCIATED CONTENT

Supporting Information. QCM-D data analysis, table S1, calculation of hydration ratio, gyration radius, interligand distant and SPR signal conversion to areal molar density. Equation S1 to S5. Supplementary Figures S1 to S11. This material is available free of charge.

AUTHOR INFORMATION

Notes

The authors declare no competing financial interests.

ACKNOWLEDGMENT

This work was partially supported by the French National Agency (ANR) under ECSTASE, Contract ANR-10-blan-1517, (Rational design of a sensitive and enantiospecific electrocatalytically-amplified aptasensor for amphetamine derivatives drugs), under ARCANE

and CBH-EUR-GS (ANR-17-EURE-0003) and the University Grenoble Alpes. The authors wish to acknowledge the support from the ICMG (FR2607) Chemistry Nanobio Platform, Grenoble. Prof. P. Labbé is acknowledged for fruitful discussions.

REFERENCES

(1) Zhou, W.; Jimmy Huang, P.-J.; Ding, J.; Liu, J. Aptamer-Based Biosensors for Biomedical Diagnostics. *Analyst* **2014,** *139*, 2627-2640.
(2) Song, S.; Wang, L.; Li, J.; Zhao, J.; Fan, C. Aptamer-Based Biosensors. *TrAC, Trends Anal. Chem.* **2008,** *27*, 108-117.
(3) Han, K.; Liang, Z.; Zhou, N. Design Strategies for Aptamer-Based Biosensors. *Sensors* **2010,** *10*, 4541.
(4) Ilgu, M.; Nilsen-Hamilton, M. Aptamers in Analytics. *Analyst* **2016,** *141*, 1551-1568.
(5) Ruan, M.; Seydou, M.; Noel, V.; Piro, B.; Maurel, F.; Barbault, F. Molecular Dynamics Simulation of a RNA Aptasensor. *J. Phys. Chem. B* **2017,** *121*, 4071-4080.
(6) Walter, J.-G.; Kökpinar, Ö.; Friehs, K.; Stahl, F.; Scheper, T. Systematic Investigation of Optimal Aptamer Immobilization for Protein−Microarray Applications. *Anal. Chem.* **2008,** *80*, 7372-7378.
(7) Martin, J. A.; Chushak, Y.; Chávez, J. L.; Hagen, J. A.; Kelley-Loughnane, N. Microarrays as Model Biosensor Platforms to Investigate the Structure and Affinity of Aptamers. *J. Nucleic Acids* **2016,** *2016*, 11.
(8) Osypova, A.; Thakar, D.; Dejeu, J.; Bonnet, H.; Van der Heyden, A.; Dubacheva, G. V.; Richter, R. P.; Defrancq, E.; Spinelli, N.; Coche-Guérente, L. *et al.* Sensor Based on Aptamer Folding to Detect Low-Molecular Weight Analytes. *Anal. Chem.* **2015,** *87*, 7566-7574.
(9) Dejeu, J.; Bonnet, H.; Spinelli, N.; Defrancq, E.; Coche-Guérente, L.; Van der Heyden, A.; Labbé, P. Impact of Conformational Transitions on SPR Signals—Theoretical Treatment and Application in Small Analytes/Aptamer Recognition. *J. Phys. Chem. C* **2018,** *122*, 21521-21530.
(10) Davis, T. M.; Wilson, W. D. Determination of the Refractive Index Increments of Small Molecules for Correction of Surface Plasmon Resonance Data. *Anal. Biochem.* **2000,** *284*, 348-353.
(11) Bornhop, D. J.; Kammer, M. N.; Kussrow, A.; Flowers, R. A.; Meiler, J. Origin and Prediction of Free-Solution Interaction Studies Performed Label-Free. *Proc. Natl. Acad. Sci. U. S. A.* **2016,** *113*, E1595-E1604.
(12) Lin, P.-H.; Yen, S.-L.; Lin, M.-S.; Chang, Y.; Louis, S. R.; Higuchi, A.; Chen, W.-Y. Microcalorimetrics Studies of the Thermodynamics and Binding Mechanism Between L-Tyrosinamide and Aptamer. *J. Phys. Chem. B* **2008,** *112*, 6665-6673.
(13) Ruta, J.; Perrier, S.; Ravelet, C.; Fize, J.; Peyrin, E. Noncompetitive Fluorescence Polarization Aptamer-based Assay for Small Molecule Detection. *Anal. Chem.* **2009,** *81*, 7468-7473.
(14) Challier, L.; Mavre, F.; Moreau, J.; Fave, C.; Schoellhorn, B.; Marchal, D.; Peyrin, E.; Noel, V.; Limoges, B. Simple and Highly Enantioselective Electrochemical Aptamer-Based Binding Assay for Trace Detection of Chiral Compounds. *Anal. Chem.* **2012,** *84*, 5415-5420.

(15) Ceretti, H.; Ponce, B.; Ramírez, S. A.; Montserrat, J. M. Adenosine Reagentless Electrochemical Aptasensor Using a Phosphorothioate Immobilization Strategy. *Electroanalysis* **2010,** *22*, 147-150.
(16) White, R. J.; Phares, N.; Lubin, A. A.; Xiao, Y.; Plaxco, K. W. Optimization of Electrochemical Aptamer-Based Sensors via Optimization of Probe Packing Density and Surface Chemistry. *Langmuir* **2008,** *24*, 10513-10518.
(17) Sandrin, L.; Thakar, D.; Goyer, C.; Labbe, P.; Boturyn, D.; Coche-Guerente, L. Controlled surface Density of RGD Ligands for Cell Adhesion: Evidence for Ligand Specificity by Using QCM-D. *J. Mater. Chem. B* **2015,** *3*, 5577-5587.
(18) Dubacheva, G. V.; Araya-Callis, C.; Geert Volbeda, A.; Fairhead, M.; Codée, J.; Howarth, M.; Richter, R. P. Controlling Multivalent Binding through Surface Chemistry: Model Study on Streptavidin. *J. Am. Chem. Soc.* **2017,** *139*, 4157-4167.
(19) Migliorini, E.; Thakar, D.; Sadir, R.; Pleiner, T.; Baleux, F.; Lortat-Jacob, H.; Coche-Guerente, L.; Richter, R. P. Well-Defined Biomimetic Surfaces to Characterize Glycosaminoglycan-Mediated Interactions on the Molecular, Supramolecular and Cellular Levels. *Biomaterials* **2014,** *35*, 8903-8915.
(20) Smith, C. L.; Milea, J. S.; Nguyen, G. H. Immobilization of Nucleic Acids Using Biotin-Strept(Avidin) Systems. In *Immobilisation of DNA on Chips Ii*, Wittmann, C., Ed. 2005; Vol. 261, pp 63-90.
(21) Rich, R. L.; Myszka, D. G. Advances in Surface Plasmon Resonance Biosensor Analysis. *Curr. Opin. Biotechnol.* **2000,** *11*, 54-61.
(22) Sauerbrey, G. Verwendung von Schwingquarzen zur Wägung Dünner Schichten und zur Mikrowägung. *Z.. Phys.* **1959,** *155*, 206-222.
(23) Reviakine, I.; Johannsmann, D.; Richter, R. P. Hearing What You Cannot See and Visualizing What You Hear: Interpreting Quartz Crystal Microbalance Data from Solvated Interfaces. *Anal. Chem.* **2011,** *83*, 8838-8848.
(24) Larsson, C.; Rodahl, M.; Höök, F. Characterization of DNA Immobilization and Subsequent Hybridization on a 2D Arrangement of Streptavidin on a Biotin-Modified Lipid Bilayer Supported on SiO2. *Anal. Chem.* **2003,** *75*, 5080-5087.
(25) Sun, L.; Svedhem, S.; Åkerman, B. Construction and Modeling of Concatemeric DNA Multilayers on a Planar Surface as Monitored by QCM-D and SPR. *Langmuir* **2014,** *30*, 8432-8441.
(26) Bingen, P.; Wang, G.; Steinmetz, N. F.; Rodahl, M.; Richter, R. P. Solvation Effects in the Quartz Crystal Microbalance with Dissipation Monitoring Response to Biomolecular Adsorption. A Phenomenological Approach. *Anal. Chem.* **2008,** *80*, 8880-8890.
(27) Thakar, D.; Migliorini, E.; Coche-Guerente, L.; Sadir, R.; Lortat-Jacob, H.; Boturyn, D.; Renaudet, O.; Labbe, P.; Richter, R. P. A Quartz Crystal Microbalance Method to Study the Terminal Functionalization of Glycosaminoglycans. *Chem. Commun.* **2014,** *50*, 15148-15151.
(28) Heinen, S.; Weinhart, M. Poly(glycidyl ether)-Based Monolayers on Gold Surfaces: Control of Grafting Density and Chain Conformation by Grafting Procedure, Surface Anchor, and Molecular Weight. *Langmuir* **2017,** *33*, 2076-2086.
(29) Pioszak, A. A.; Parker, N. R.; Gardella, T. J.; Xu, H. E. Structural Basis for Parathyroid Hormone-related Protein Binding to the Parathyroid Hormone Receptor and Design of Conformation-selective Peptides. *J. Biol. Chem.* **2009,** *284*, 28382-28391.
(30) Grauschopf, U.; Lilie, H.; Honold, K.; Wozny, M.; Reusch, D.; Esswein, A.; Schäfer, W.; Rücknagel, K. P.; Rudolph, R. The N-Terminal Fragment of Human Parathyroid Hormone

Receptor 1 Constitutes a Hormone Binding Domain and Reveals a Distinct Disulfide Pattern. *Biochemistry* **2000,** *39*, 8878-8887.
(31) Lin, P.-H.; Chen, R.-H.; Lee, C.-H.; Chang, Y.; Chen, C.-S.; Chen, W.-Y. Studies of the Binding Mechanism Between Aptamers and Thrombin by Circular Dichroism, Surface Plasmon Resonance and Isothermal Titration Calorimetry. *Colloids and Surfaces B: Biointerfaces* **2011,** *88*, 552-558.
(32) Chang, A. L.; McKeague, M.; Liang, J. C.; Smolke, C. D. Kinetic and Equilibrium Binding Characterization of Aptamers to Small Molecules using a Label-Free, Sensitive, and Scalable Platform. *Anal. Chem.* **2014,** *86*, 3273-3278.
(33) Flores, C.; Woodbury, N. W.; Katilius, E. Exploring the Sequence Space of a DNA Aptamer Using Microarrays. *Nucleic Acids Res.* **2007,** *35*, 7626-7635.
(34) Collett, J. R.; Cho, E. J.; Ellington, A. D. Production and Processing of Aptamer Microarrays. *Methods* **2005,** *37*, 4-15.
(35) Jung, L. S.; Campbell, C. T.; Chinowsky, T. M.; Mar, M. N.; Yee, S. S. Quantitative Interpretation of the Response of Surface Plasmon Resonance Sensors to Adsorbed Films. *Langmuir* **1998,** *14*, 5636-5648.
(36) Liang, D. H.; Luu, Y. K.; Kim, K. S.; Hsiao, B. S.; Hadjiargyrou, M.; Chu, B. In Vitro Non-Viral Gene Delivery With Nanofibrous Scaffolds. *Nucleic Acids Res.* **2005,** *33*.
(37) Lai, E.; van Zanten, J. H. Monitoring DNA/poly-L-Lysine Polyplex Formation with Time-Resolved Multiangle Laser Light Scattering. *Biophys. J.* **2001,** *80*, 864-873.
(38) Tumolo, T.; Angnes, L.; Baptista, M. S. Determination of the Refractive Index Increment (dn/dc) of Molecule and Macromolecule Solutions by Surface Plasmon Resonance. *Anal. Biochem.* **2004,** *333*, 273-279.
(39) Gestwicki, J. E.; Hsieh, H. V.; Pitner, J. B. Using Receptor Conformational Change to Detect Low Molecular Weight Analytes by Surface Plasmon Resonance. *Anal. Chem.* **2001,** *73*, 5732-5737.
(40) Dell'Orco, D.; Muller, M.; Koch, K. W. Quantitative Detection of Conformational Transitions in a Calcium Sensor Protein by Surface Plasmon Resonance. *Chem. Commun.* **2010,** *46*, 7316-7318.

TOC GRAPHICS